Aerospace Science and Technology 174 (2026) 111785

Contents lists available at ScienceDirect

Aerospace Science and Technology

journal homepage: www.elsevier.com/locate/aescte

Vehicle envelope with lightweight ultrafilm for minimal leakage (VELUM) ⋆

Afsaneh Kheirani [a,b,1], Ilyass Tabiai [a,c], David St-Onge [a,b,*]

[a] Department of Mechanical Engineering, École de Technologie Supérieure (ÉTS), 1100 Notre-Dame St W, Montreal, QC, Canada
[b] INIT Robots Lab, École de Technologie Supérieure (ÉTS), 1100 Notre-Dame St W, Montreal, QC, Canada
[c] CREPEC, Research Center for High Performance Polymer and Composite Systems, Canada

ARTICLE INFO

Communicated by Dr Mehdi Ghoreyshi

Keywords:
Indoor airship
Inflatable structures
Semi-rigid airship
Gas barrier membrane
Thin polymer film
LDPE film
Sol gel coating

ABSTRACT

Indoor inspection and mapping missions in tunnels, industrial facilities, and subterranean environments require aerial platforms capable of long-duration operation in cluttered, humid, and navigation-denied conditions. While multirotor drones provide high maneuverability, their endurance and payload capacity are fundamentally limited by battery-powered lift. Small indoor lighter-than-air vehicles alleviate this constraint through buoyancy; however, at meter-scale volumes, envelope materials become a critical limitation, as they largely determine system mass, gas retention, durability, and resistance to handling and collisions. Commonly used films present persistent trade-offs: metallized polyester offers low gas permeability but limited mechanical robustness, whereas polyurethane is more durable but heavier and more permeable.

This work introduces and experimentally validates a lightweight composite envelope material based on low-density polyethylene combined with a fluoro-siloxane barrier coating. The proposed treatment significantly improves helium retention while preserving flexibility and resistance to handling. Mechanical and functional testing show that the coated material achieves substantially higher tear resistance than metallized polyester and improved durability compared to polyurethane, while remaining considerably lighter. A cylindrical airship fabricated from this membrane was deployed in a semi-autonomous underground mapping mission, demonstrating reduced helium leakage, stable performance in humid conditions, and multi-day operation. These results show that fluoro-siloxane-coated polyethylene enables lightweight, durable, and gas-efficient envelopes, supporting persistent indoor operation of small lighter-than-air aerial platforms.

1. Introduction

Mobile robots are increasingly deployed for inspection, mapping, scientific exploration, and safety-critical operations in environments where direct human intervention is hazardous or impractical [1,2]. Recent advances in sensing, autonomy, communication, and multi-robot coordination have broadened their use across industrial, civil, and scientific domains, with comprehensive surveys highlighting rapid progress in navigation, perception, swarm coordination, and task automation, particularly for indoor and infrastructure-focused applications [1,2]. As a result, aerial mobile robots are now routinely considered for missions in complex and previously inaccessible spaces [1].

In confined indoor environments, multirotor drones remain the dominant aerial platform due to their agility, maneuverability, and precise hovering capability [3,4]. They are widely employed in industrial facilities and warehouses [3], tunnels [5], and archaeological or heritage sites [4,6], as well as in subterranean settings such as caves, mines, and underground infrastructures where uneven, flooded, or unstable terrain can render terrestrial robots ineffective [7,8]. Despite substantial advances in autonomy and control, these environments expose a fundamental limitation of multirotor systems: their reliance on continuous, battery-powered thrust to generate lift [1].

Recent work has primarily addressed this limitation through system- and control-level strategies, including improved navigation,

⋆ This work is the subject of an international patent application (PCT/CA2025/050918), entitled “Aerostat envelope, aerostat comprising same, and method of manufacturing same,” filed July 2, 2025, by École de technologie supérieure. Inventors: A. Kheirani, D. St-Onge, I. Tabiai, and N. Tepylo.

Abbreviations: CAD, Computer-aided design; CA, Static water contact angle; EVOH, Ethylene vinyl alcohol copolymer; GPS, Global Positioning System; HDPE, High-density polyethylene; He, Helium; LLDPE, Linear low-density polyethylene; LDPE, Low-density polyethylene; LTA, Lighter-than-air; MFI, Melt flow index; MTS, Mechanical testing system (MTS Alliance RF/200); PU, Polyurethane; PVDC, Polyvinylidene chloride; RF, Radio-frequency; VCA, Video contact angle (system).

* Corresponding author.
E-mail addresses: afsaneh.kheirani.1@ens.etsmtl.ca (A. Kheirani), Ilyass.tabiai@etsmtl.ca (I. Tabiai), David.st-onge@etsmtl.ca (D. St-Onge).

[1] Additional information: VELUM project (materials and methods details), Project website (Real deployments).

https://doi.org/10.1016/j.ast.2026.111785
Received 23 October 2025; Received in revised form 15 January 2026; Accepted 26 January 2026
Available online 9 February 2026

Nomenclature

ρ g/cm^3	Density
t mm	Film thickness
σ MPa	Tensile stress
P kPa	Internal pressure
$\dot{m}_{He}$ g/h	Helium leakage rate
V m^3	Envelope volume

energy-aware planning, swarm coordination [1,9], and real-time mass and inertia estimation [10], in an effort to extend mission capability without modifying the underlying multirotor architecture. Although such approaches can increase the efficiency with which onboard energy is used, they do not remove the basic requirement for sustained propulsive lift. Consequently, limited flight time and restricted payload margins remain critical bottlenecks for indoor and long-duration missions, particularly in GPS-denied, humid, or geometrically constrained environments [1].

To overcome these constraints, Lighter-than-air (LTA) vehicles offer an alternative aerial paradigm by exploiting buoyant lift to sustain flight with minimal energy expenditure. By decoupling lift generation from continuous power consumption, LTA platforms directly address the endurance limitations inherent to multirotor systems. Their low noise, reduced vibration, and low-impact dynamics make them particularly well suited for sensitive or confined environments, while their inflatable structure enables lightweight construction, mechanical robustness, and compact storage [11,12].

Although lighter-than-air vehicles have traditionally been used for entertainment and advertising, several research prototypes have demonstrated their feasibility for scientific and robotic applications [13–16], including operation in underground or tunnel-like environments [17, 18]. These efforts confirmed the potential of small-scale LTA platforms for persistent aerial operation, while also revealing significant technical challenges. Multiple avenues have been explored to address these limitations, including refinements in vehicle geometry, control strategies, hybrid buoyant-propulsive configurations, and adaptive or compliant structures. However, at the indoor scale of roughly one cubic meter –compatible with doorways and confined passages– the envelope material remains a first-order system constraint. The limited lifting-gas volume leaves very narrow mass margins once essential onboard components such as actuators, sensors, and processing units are accounted for [7]. As a result, the envelope often dominates the mass budget, in some designs accounting for more than 30% of the available lift [15,18]. These material-level constraints bound achievable performance regardless of higher-level control or structural strategies, making envelope materials a critical and comparatively underexplored design dimension for persistent indoor LTA operation.

Existing materials such as Mylar and polyurethane (PU) involve fundamental compromises: the former offers low permeability but suffers from brittleness, while the latter provides flexibility at the expense of weight and gas retention. These persistent trade-offs indicate that neither material provides a fully balanced combination of mechanical robustness, mass efficiency, and gas retention for repeated field deployment in confined environments, motivating the exploration of alternative envelope materials.

Low-density polyethylene (LDPE) has recently emerged as a promising candidate in this context due to its favorable mechanical behavior and low areal density; however, its relatively high gas permeability remains a limiting factor for long-duration missions.

Accordingly, the objective of this work is to develop and experimentally validate a lightweight envelope material that reconciles mechanical robustness, mass efficiency, and gas retention for small indoor LTA vehicles. To this end, the study (i) quantitatively characterizes the mechanical and functional limitations of commonly used PU and Mylar membranes, (ii) evaluates LDPE as a mechanically advantageous alternative, (iii) addresses its remaining permeability limitation through a lightweight surface treatment, and (iv) validates the resulting material through laboratory testing and full-scale field deployment in a confined underground environment.

The remainder of the paper is structured as follows. Section 2 defines the performance requirements for indoor airship membranes, Section 3 describes the materials and experimental methods, Section 4 details the fabrication of laboratory and full-scale envelopes, Section 5 presents the experimental results, and Section 6 reports on field deployment.

2. Background: Membrane performance

While most LTA research has focused on autonomy and platform-level integration, less attention has been given to the envelope materials that determine sustained indoor operation. The following criteria provide a framework for evaluating candidate materials, capturing requirements that must be simultaneously satisfied for the efficient operation of both large- and small-scale LTA systems [19,20]:

- **High specific strength:**[1] The material should be lightweight to maximize payload while providing tensile strength under biaxial stress to resist pressurization loads, attachment forces, and handling stresses. Adequate strength reduces creep, permanent deformation, and rupture, preserving envelope stability during long-term operation.
- **Tear resistance:** Resistance to tear initiation and propagation is critical, as small cuts or stress concentrators may develop under bending, snagging, or folding [21,22]. Whether defects remain stable depends on their size, material toughness, and in-service stresses (e.g., internal pressure, biaxial tension, environmental effects). In large outdoor airships, sub-critical slits may only cause slow leaks, allowing mooring [23] and repair, whereas for small indoor vehicles, even minor leaks can terminate a mission. Complementary burst tests reveal thresholds beyond which cracks propagate rapidly under biaxial loading. Failure mode depends on toughness: brittle films fragment into multiple tears, while tougher films fail as a localized slit. Thus, adequate tear resistance is required both to prevent gradual lift loss and to avoid catastrophic rupture.
- **Puncture resistance:** The material must withstand concentrated forces without penetration, protecting against sharp objects during handling and in-flight collisions, a common risk indoors.
- **High gas barrier properties:** Low helium permeability is essential for maintaining flight duration and reducing operational costs. Helium permeability, expressed in cm^3·mm/m^2·day·atm, quantifies the diffusion of helium through a standardized membrane area and thickness over 24 hours at one atmosphere. Lower values indicate stronger barrier performance. While most untreated polymer films exhibit relatively high helium permeability compared to advanced barrier materials, surface modifications and nanocomposite coatings can significantly reduce gas transmission by extending diffusion pathways and lowering free volume [24–27].
- **Wettability and moisture resistance:** Wettability, which determines a material's hydrophobic or hydrophilic behavior, depends on chemical composition and surface morphology; rough, low-energy surfaces promote water repellency. The degree of wettability is commonly quantified by the *static water contact angle* (CA), defined as the angle between the tangent to a liquid droplet at the solid-liquid-vapor interface and the solid surface. Hydrophilic surfaces exhibit CA values below 90°, whereas hydrophobic surfaces show CA values greater than 90°. Superhydrophobicity requires CA values above 150° [28]. These surface properties mitigate moisture uptake [29], which would otherwise increase mass and compromise the mechan-

[1] Often defined in mechanics as *specific tensile strength* (strength divided by density). In aerospace and LTA literature, the equivalent concept is more commonly referred to as "strength-to-weight ratio" [19,20].

ical consistency, thereby reducing the endurance and reliability of the envelope material.

- **Welding test:** Welding of polymers through the application of heat enables lightweight, strong joints without adhesives or mechanical fasteners, minimizing both weight and fabrication complexity. Thermal bonding is also necessary for unconventional envelope geometry, as heat welding allows continuous, airtight seams along complex curvatures. Industrial envelopes are generally limited to standard shapes and sizes, and custom manufacturing is often unavailable or prohibitively expensive.
- **Cost-effectiveness and maintenance:** Economically viable materials that can be repaired easily are essential for extending service life and reducing maintenance.

Among these factors, high specific strength and gas barrier properties are the most critical for indoor use due to the tight size and payload constraints. Single-layer films are lightweight but rarely satisfy all requirements simultaneously. Consequently, two complementary strategies are widely used [11,19,20,30]: *lamination*, which integrates gas-barrier layers between structural plies to extend diffusion paths and improve tear resistance; and *surface coating*, which fills micro-voids and reduces free volume to suppress helium transport.

Recent outdoor-focused research has advanced multi-layer laminates and high-performance fibers. Li et al. [19] achieved permeability below 0.1 $cm^3 \cdot mm/m^2 \cdot day \cdot atm$ using Zylon® and Vectran® textiles with aluminum coatings, combining excellent barrier and UV resistance. Chouhan et al. [30] and Joshi et al. [26] developed coated laminates with high durability, but such systems require complex fabrication and add weight, making them unsuitable for small-scale indoor LTA applications. Dhawan and Jindal [20] improved PU laminates with fabric reinforcement, though at the cost of higher surface density. PU nanocomposites with graphene or layered silicates [31] reduce gas diffusion but demand precise dispersion control, increasing cost.

Other barrier polymers, including Mylar®, EVOH, and PVDC, have very good gas retention but poor low-temperature flexibility and sealability, and they can crack under repeated loading [26,31]. EVOH-based laminates, for example, can reach permeabilities as low as 0.04–0.8 $cm^3\,mm/m^2\,day\,atm$ and surface densities of about 103–113 g/m^2 [27], but they are optimized for outdoor conditions and are unnecessarily complex for indoor use.

In practice, compact indoor LTAs rely mostly on commercially available PU and Mylar® films [32,33].
Both materials present clear drawbacks. Mylar provides low permeability but is brittle and prone to failure under repeated folding, often requiring additional protective layers that offset weight savings [34]. PU offers flexibility and durability but suffers from high helium permeability due to its copolymer microstructure; heavier grades improve retention but at the expense of mass [31].

While helium is the primary lift gas, O_2 (atomic radius 0.35 nm) and CO_2 (atomic radius 0.33 nm) permeabilities are commonly measured as proxies, since diffusion follows the solution-diffusion model, where both molecular size and gas solubility in the polymer govern transport [11,20,31]. Table 1 summarizes reported permeabilities of common LTA films and advanced barrier materials. PU exhibits the highest helium permeability, whereas Mylar achieves substantially lower values. EVOH and PVDC demonstrate the strongest barrier performance across all gases [31]; however, their use in indoor LTA systems is limited by moisture sensitivity, thermal instability, and poor weldability [35,36]. Along with the higher basis weights required for durability, these drawbacks limit their practicality in lightweight indoor envelopes.

Given these limitations, this study investigated low-density polyethylene (LDPE) as a lightweight, tear-resistant alternative for indoor airship envelopes. LDPE is flexible, impact-resistant, and lighter than PU, while offering better tear resistance than Mylar®. However, its amorphous structure contains free-volume voids that allow helium diffusion (atomic radius 0.26 nm) [11,37]. Despite this, LDPE exhibits lower O_2 and CO_2 permeability than PU [31], suggesting potential for improved helium retention. To address its intrinsic helium permeability, lightweight surface coatings and nanostructured fillers were investigated to reduce free volume and introduce tortuous diffusion pathways [24,38].

Table 1
Gas permeability of different polymeric/elastomeric film materials used for LTA envelope applications at standard testing conditions [31,39].

Polymer/Elastomer	Permeability ($cm^3 \cdot mm/m^2 \cdot day \cdot atm$)		
	O_2	CO_2	He
PU	3–1067	175–2014	36–2340
Mylar®	1–2.4	5.9–8.9	71
EVOH	0.01–0.05	0.03–0.08	4–14
PVDC	0.03–0.04	0.47–3.2	–
LDPE	69–274	394–959	–

3. Materials and methods

Potential candidate polymers for indoor LTA envelopes were studied through a series of mechanical and functional tests. The selected tests provided a comprehensive evaluation of membrane performance under conditions relevant to indoor LTA operation. Mechanical tests (tear, puncture, tensile, and burst) captured structural integrity and failure modes under localized and distributed loads, while functional tests (gas barrier, hydrophobicity, and thermal bonding) addressed envelope durability, lift retention, and manufacturability. Together, these methods established a consistent basis for comparing LDPE against conventional PU and Mylar membranes and for identifying trade-offs between mass efficiency, mechanical robustness, and gas retention.

LDPE is a widely used thermoplastic distinguished by its toughness, chemical resistance, and ease of processing. Within the polyethylene family, its highly branched molecular structure and broad weight distribution provide greater softness and flexibility than linear low-density polyethylene (LLDPE) and high-density polyethylene (HDPE) [40,41]. These characteristics make LDPE particularly suitable for lightweight films requiring sealability and ease of fabrication. A commercial-grade LDPE was sourced [42] and characterized with a Melt Flow Index (MFI) of 2.66 ± 0.12 g/10 min, measured according to ASTM D1238, Method A [43] (six samples, KAYJAY/2006/AC, 230 °C, 2.16 kg load).

3.1. Density and thickness measurements

Envelope mass is a critical design parameter; therefore, most results were reported relative to material density. Density was measured using a helium pycnometer (Micromeritics/Folio Instruments, AccuPyc 1340) with ten repetitions per sample. Helium was selected for its small atomic radius, which enables penetration into micro-voids and the accurate determination of true film volume. Film thickness was measured with a digital micrometer (0.001 mm resolution) at five distinct locations to capture potential heterogeneity.

3.2. Tear test

Tear resistance was measured according to ASTM D1004 [44] on an MTS Alliance RF/200 machine. Double-notch specimens were prepared using a Kongsberg X24 Edge cutting system (geometry shown in Fig. 1). Tests were conducted in Mode III (anti-plane shear) [45], replicating tear initiation in envelopes subjected to snagging, bending, or uneven inflation. One grip remained fixed while the other displaced at 51 mm/min (2 in/min). A 100 N load cell (electrical sensitivity: 1.95 mV/V; resolution:0.01 N) recorded force-displacement curves for quantitative assessment. For statistical reliability, four specimens were tested for each material. LDPE films may exhibit direction-dependent

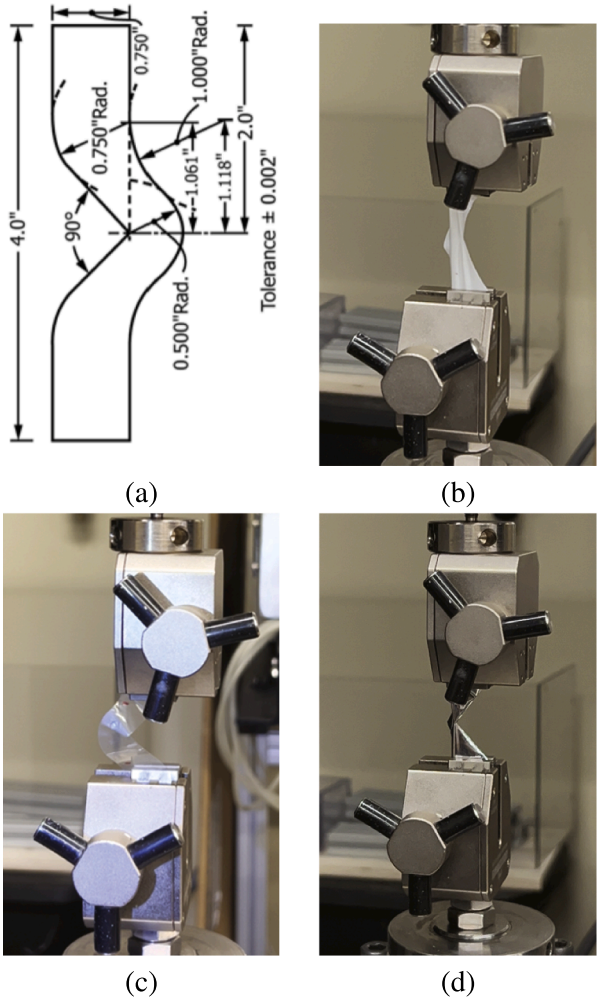

Fig. 1. Tear test methodology: (a) Double-notch specimen geometry prepared in compliance with ASTM D1004 standards. Experimental setup for evaluating tear resistance in (b) PU film, (c) LDPE film, and (d) Mylar film.

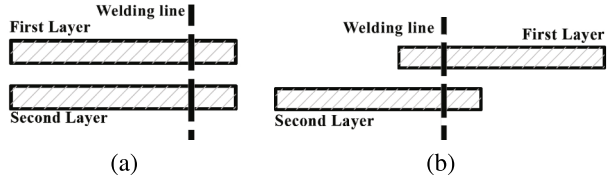

Fig. 2. Joint configurations used in the sealed-joint tensile tests (ASTM F88/F88M-21): (a) T1, superimposed joint configuration; (b) T2, flap joint configuration. These labels (T1 and T2) are used throughout the paper to identify the tensile test configuration.The figure presents visual representations of these two joint configurations, which are commonly used in structural applications. Understanding the differences between these joint types is essential for selecting appropriate joining methods in engineering design.

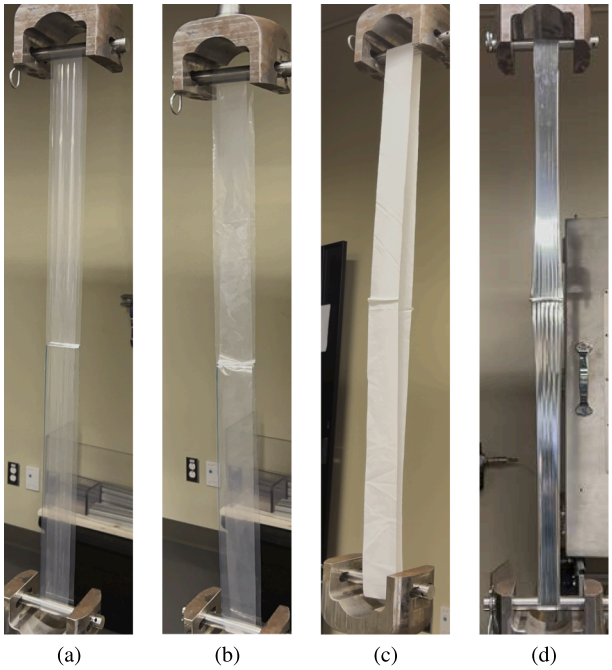

Fig. 3. Representative tensile specimens prepared according to ASTM F88/F88M-21, showing the tested material–configuration combinations: (a) LDPE, configuration T1 (superimposed joint); (b) LDPE, configuration T2 (flap joint); (c) PU, configuration T1; (d) Mylar, configuration T1. Only LDPE was tested in both configurations (T1 and T2) to isolate the effect of joint geometry.

tearing behavior due to processing-induced molecular orientation. During preliminary calibration trials, qualitative differences in tear propagation were observed when specimens were aligned along different in-plane directions. However, specimen orientation was not systematically controlled in the present test campaign. Accordingly, the reported tear results are provided without directional separation.

3.3. Puncture test

Puncture resistance was evaluated according to ASTM F1306 [46] using the same MTS system. A hemispherical 3.2 mm plunger was driven at 25 mm/min into specimens (51 ×76 mm) clamped over a 34.9 mm hole. Four replicates were tested per material. A 100 N load cell (electrical sensitivity: 1.95 mV/V; resolution:0.01 N)recorded force-displacement curves for quantitative assessment. For statistical reliability, four specimens were tested for each material.

3.4. Tensile strength of sealed joints

Sealed-joint tensile strength was assessed using two predefined joint configurations for LDPE, denoted as T1 (superimposed joint) and T2 (flap joint), while PU and Mylar were tested only in the T1 configuration (Fig. 2). Loop samples, 50 mm wide, were sealed on both edges following ASTM F88/F88M-21 [47]. Testing was performed on the same MTS RF/200 machine with cylindrical grips to minimize stress concentrations, using a 1000 N load cell (electrical sensitivity: 2 mV/V; resolution: 0.0005 N) and a crosshead speed of 200 mm/min. Maximum load and displacement at failure were recorded for four repeated tests (Fig. 3).

3.5. Gas barrier test

Gas barrier performance was evaluated through full-envelope helium retention, rather than localized permeation measurements (e.g., N500 [48]). This system-level approach captured the combined effects of polymer permeability, seam integrity, and geometry. It aligned with practices used in high-altitude balloon development, such as Loon LLC's stratospheric platforms [49] and Venus balloon prototypes [50].

Custom pillow-shaped envelopes of identical dimensions were fabricated: LDPE envelopes were produced and coated in-house, while PU and Mylar envelopes were sourced commercially. Each envelope was inflated to 4 kPa with helium and suspended from a 50 N load cell (Fig. 4). Internal pressure was monitored with a differential sensor

Table 2
Initial weights of LDPE, PU, and Mylar pillows for gas barrier evaluation.

Pillow Size (mm)	Material	Pillow Weight (g)
800 × 1200	Mylar	57
	PU	131.22
	Non-Coated LDPE	124.15
	Coated LDPE	128.2

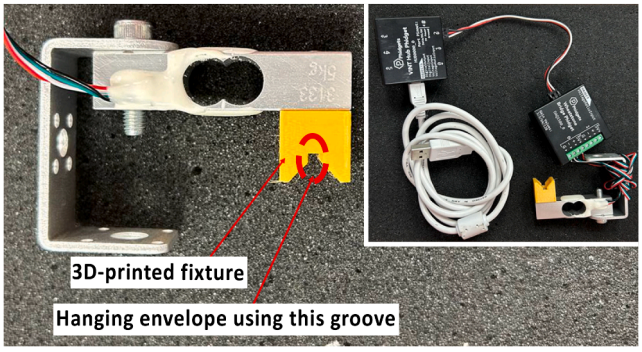

Fig. 4. Schematic of load cell setup for helium leakage performance measurement in pillow-shaped samples. The load cell measured the lift force exerted by the pillow, which correlated with internal helium pressure and retention.

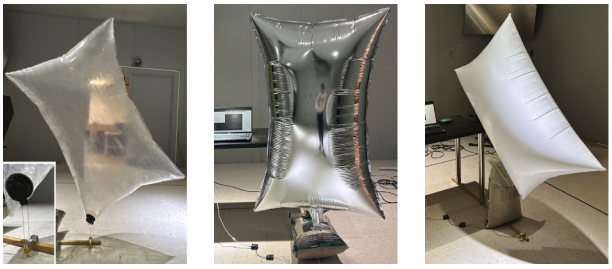

Fig. 5. Gas barrier comparison of pillows made from (a) LDPE film, (b) Mylar film, and (c) PU film. All pillows had identical dimensions and were tested under the same conditions, inflated to the same internal pressure, and placed in a temperature-controlled, isolated room with minimal airflow or external disturbances (e.g., airflow or motion caused by nearby personnel).

(±25 kPa, Phidgets 1126_0)[2]). Lift was tracked at 1.5-minute intervals for six hours in a sealed room at 26-27 °C, with the first 10 minutes excluded to eliminate manipulation disturbances, including effects associated with manual suspension of the envelope, residual oscillations of the load-cell system, and short-term air disturbances immediately following release (Fig. 5). For each material, the helium retention test was repeated three times using independently fabricated envelopes. All tests were conducted in an isolated room with minimal airflow to ensure that subsequent measurements reflected steady-state helium leakage rather than external mechanical disturbances. Initial envelope weights were recorded and are reported in Table 2.

Durability was assessed by subjecting each deflated sample to 30 minutes of tumble agitation (air-fluff, no heat, two wool dryer balls), followed by reinflation and repetition of the helium retention protocol.

3.6. Wettability properties

Wettability was assessed via static contact angle using a VCA Optima Video Contact Angle System,[3]) following the sessile drop method. Samples (30 × 30 mm) were cleaned with compressed air before droplet deposition. A syringe filled with distilled water was used to dispense droplets onto the sample surfaces, and four measurements per specimen were taken across different locations. Average contact angle and standard deviation were computed.

3.7. Thermal welding

Thermal welding trials were performed on LDPE, PU, and Mylar films using a manually actuated heat roller. Temperature was increased in 5-10 °C increments to identify welding temperature ranges that produced continuous, defect-free welds. The vertical load was estimated using a digital balance placed under the roller. After cooling, the welds were visually inspected for wrinkling, curling, or incomplete fusion to assess weld quality. The mechanical strength of the welded joints was subsequently evaluated through dedicated tests, as described in 5.4. Identifying the appropriate welding temperature for each material was necessary to balance weld strength and film integrity. Excessively low temperatures resulted in incomplete fusion and weak, leak-prone joints, whereas overly high temperatures caused the membrane to thin or perforate, creating microscopic holes or thermal damage along the weld line. In this study, optimal thermal welding was defined as the temperature range that produced continuous welds without visible defects and yielded the highest joint strength in tensile testing. Determining this range ensured strong, continuous welds without compromising the structural or barrier properties of the film.

3.8. Validation of burt behavior

Burst resistance was assessed through inflation-to-failure tests, capturing biaxial stress response, tear propagation, and rupture mode [51–53].

Pillow-shaped envelopes (800 × 1200 mm) were thermally welded and inflated with compressed air until rupture. Compressed air was used instead of helium because rupture pressure and failure behavior are governed by internal pressure and the resulting biaxial membrane stress, which are independent of the gas types at identical pressure levels. The objectives were to determine: (i) maximum internal pressure, (ii) rupture location (film vs. seal), and (iii) pressure-time behavior under biaxial loading.

Pressure was measured at 10 Hz using a differential sensor (±25 kPa range, 55 Pa resolution). Rupture events were recorded on video to document failure modes. One specimen per material ($n = 1$) was tested due to resource constraints, providing representative comparative data despite limited statistical robustness.

4. Fabrication of coated LDPE membranes

To overcome the limitations of conventional PU and Mylar films in indoor LTA applications, a custom in-house fabrication protocol was developed for coated LDPE envelopes, enabling systematic evaluation of material performance under representative operating conditions. The fabrication process was designed to maximize helium retention while maintaining gas-tightness, tear resistance, flexibility, and low mass. The sequential steps were outlined in Fig. 6 and are described below.

4.1. Gore preparation

The number and arrangement of gores[4] were selected according to the target geometry and fabrication requirements. The gore layout balanced two competing factors: minimizing the number of welds to reduce

[2] www.Phidgets.com
[3] www.astp.com

[4] In this study, *gores* refer to the individual membrane panels thermally welded to form the main envelope body.

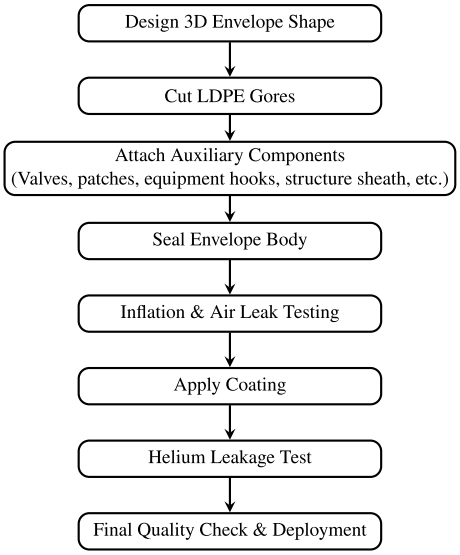

Fig. 6. Flowchart illustrating the LDPE airship envelope fabrication process used in this study. The figure outlines the sequential steps involved, from the initial design of the envelope shape to the final quality check and deployment.

leakage risk and ensuring geometric conformity after assembly. For symmetric or moderate-scale envelopes, two-gore configurations (e.g., pillow or cylindrical shapes) reduced fabrication complexity and leakage probability. Multi-gore designs provided better conformity for elongated or complex geometries but increased the number of welds, raising alignment and thermal welding demands.

Gore layouts were derived by flattening the 3D surface model of the envelope in CAD software (SolidWorks in this work). In addition to gores, *patches* were thermally welded locally to reinforce mounting points for structural components (e.g., carbon tubes), distributing concentrated loads without compromising gas-tightness. Gores were cut either manually or using a digital cutting system (Kongsberg X24 Edge in this work), the latter ensuring high precision and repeatability for prototypes.

4.2. LDPE envelope thermal welding

Thermal welding was a critical step, particularly for complex geometries where curved weld seams or sharp transitions prevented the membrane from lying flat. Each gore was positioned over a rigid support, either flat on the table or on a fixture shaped to the envelope cross-section, ensuring alignment during thermal welding. Strong, airtight weld seams required uniform seam width, precise temperature control, and consistent pressure application.

Welding was performed using a heat roller with integrated digital temperature regulation (Fig. 7(a)). During welding, heat was supplied by the roller element, while pressure was applied manually by the operator through downward force on the roller along the weld seam. Compared to radio-frequency (RF) welding, which relies on dielectric heating [30,48,54], the heat-roller method enabled continuous thermal welding over long weld seams, accommodated non-uniform geometries, and was more cost-effective. During preliminary trials, the roller temperature was adjusted in discrete increments of 5-10 °C to identify a processing window that produced continuous, defect-free weld seams without film thinning or perforation. For LDPE, optimal thermal welding was achieved at a roller temperature of 170 °C.

A silicone mat was placed beneath the film to improve weld quality. Welding offsets (10 mm, corresponding to the roller tip width) were aligned and secured with tape or grippers. A silicone-coated parchment barrier prevented sticking. The applied pressure was generated by the operator through controlled manual force on the roller. The magnitude of this force was measured before welding by applying the roller onto a digital balance, corresponding to an equivalent load of approximately 300 g. During welding, the operator maintained a comparable pressure level guided by this reference. The adequacy and consistency of the applied pressure were verified indirectly through the uniformity, continuity, and repeatability of the resulting weld seams. Under these conditions, a uniform welded joint approximately 5 mm wide (corresponding to the roller tip width) was consistently produced.

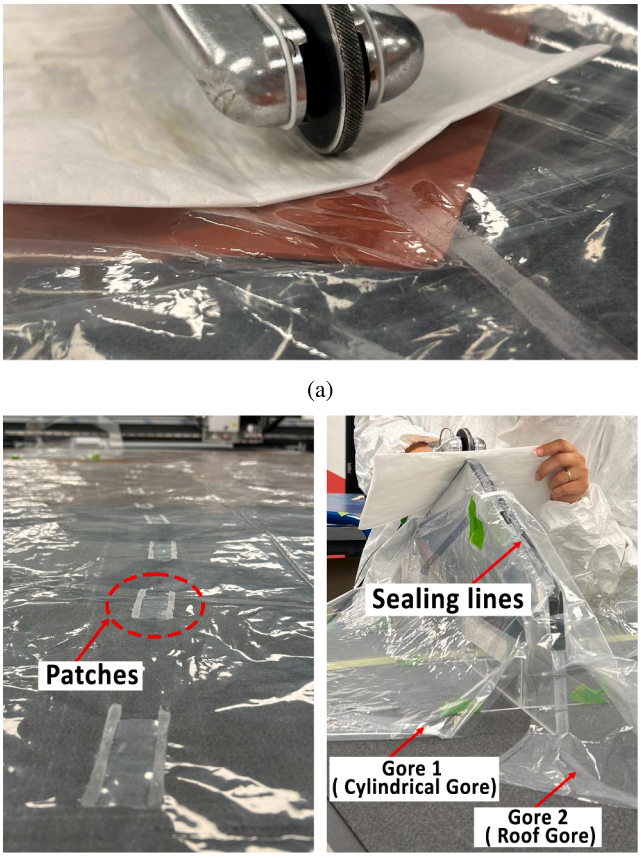

Fig. 7. Components and setup for the envelope fabrication process: (a) Heat roller and mattress for thermal welding of gores and auxiliary components; (b) Thermally welded patches; (c) Envelope thermal welding using a custom-made fixture.

Auxiliary components such as valves, sensor mounts, and structural patches (Fig. 7(b)) were pre-attached before envelope assembly. For simple two-gore designs, a sequential thermal welding approach was used. More complex geometries (e.g., cylindrical bodies with end caps [55]) required custom fixtures to stabilize multi-gore intersections (Fig. 7(c)). Heat-resistant silicone mats were used on top surfaces to prevent deformation and protect the polycarbonate fixtures. Following assembly, each envelope was inflated and monitored for 24 h to confirm leak-free, gas-tight performance.

4.3. Surface coating

After verifying air-tightness, envelopes were coated while inflated using an “under-load” technique. This approach prevented voids caused by material stretching during subsequent pressurization and ensured uniform surface coverage. Coating was applied only after all seams were welded, since applying it beforehand would have prevented the film layers from bonding during thermal welding.

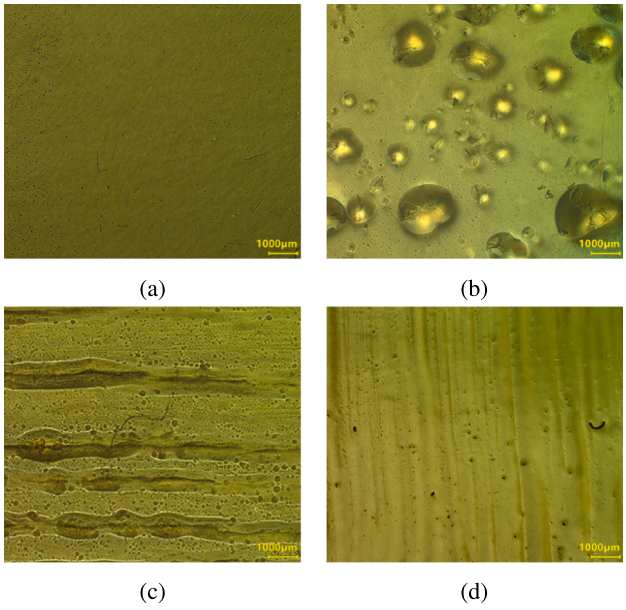

Fig. 8. Surface morphology of LDPE samples observed with a VHX-7000 digital microscope: (a) non-coated surface, (b) after spraying, (c) after wiping, and (d) after spray-wipe coating. The spray-wipe method produced the most homogeneous and defect-free layer.

Three application methods were compared:

1. *Spraying:* a high-pressure spray gun ensured broad coverage but produced discontinuous layers with droplet clustering.
2. *Wiping:* nanofiber cloths distributed the coating manually, improving uniformity but leaving localized voids.
3. *Spray-wipe:* spraying provided initial coverage, followed by wiping to redistribute droplets into a continuous film. This hybrid method produced the smoothest, most homogeneous layer with strong adhesion.

Surface morphology was analyzed with a digital microscope (VHX-7000) on samples extracted from central, edge, and seam-adjacent zones. Non-coated LDPE (Fig. 8(a)) exhibited micro-voids and irregularities acting as leakage pathways. Spray-only coatings (Fig. 8(b)) showed macro-particles, micro-cracks, and particle clustering; wiping alone (Fig. 8(c)) improved coverage but retained voids. The combined spray-wipe method (Fig. 8(d)) achieved the most homogeneous, defect-free coating.

For coating, the inflated envelope was suspended in a rigid carbon-tube frame to prevent contact between the membrane and external surfaces (e.g., ground or supports). Suspension ensured unobstructed access to the entire envelope surface, enabling uniform coating coverage while avoiding local deformation or non-uniformity in coating during application and curing. The frame also provided mechanical support for handling and repositioning. Before coating, the surface was cleaned using an alcohol-based solution sprayed at 5-6 bar from a distance of 500 mm, followed by wiping with microfiber cloths after a 2 min evaporation period.

The coating procedure consisted of three steps:

1. *Spraying:* the fluoro-siloxane sol-gel coating was applied with two passes at 5-6 bar and a 500 mm spray distance.
2. *Wiping:* after one minute of settling, the surface was wiped unidirectionally with a microfiber cloth lightly dampened with the coating solution to redistribute droplets and eliminate streaks. The coating entered a gel-like state within 10-15 min, requiring rapid execution.
3. *Curing:* the coated envelope was cured for 48 h under ventilation at 25 ± 1 °C. During curing, the surfaces became rougher and slightly opaque, consistent with surface modifications reported in plasma-treated LDPE films [56,57].

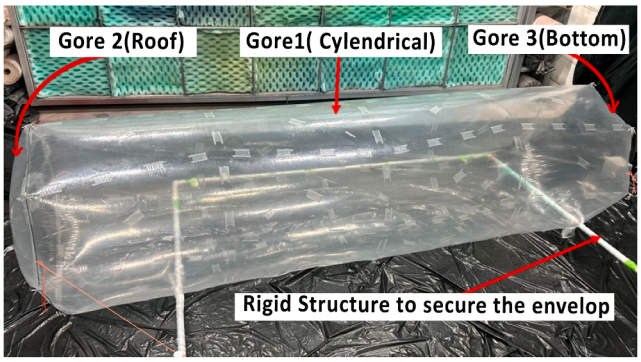

Fig. 9. Coated envelope. The figure illustrates the main steps and resulting appearance of the coating.

Table 3
Physical properties of selected materials: Mylar (silver), PU (white), and LDPE pure / coated (transparent). Reported density values correspond to mean values obtained from helium pycnometry (ten repetitions per sample; standard deviations were 0.0065, 0.0160, and 0.0044 g/cm^3 for Mylar, PU, and LDPE, respectively), and thickness was determined with a digital micrometer (0.001 mm device resolution, five measurements per sample). All measurements were conducted at ambient temperature (about 25 °C).

Material	Density (g/cm^3)	Thickness (mm)	Surface dens. (g/m^2)
Mylar	1.0783	0.025	27.60
PU	1.3365	0.052	70.00
LDPE (Pure)	0.9674	0.049	48.00
LDPE (Coated)	0.9636	0.056	54.54

The final coated LDPE envelope, suspended within its frame, is shown in Fig. 9.

The fabrication process yielded repeatable, defect-free coated LDPE envelopes that combined lightweight construction with enhanced gas retention, providing consistent test specimens for the performance evaluations presented in the following section.

5. Results and discussion

This section presents a comparative evaluation of LDPE, PU, and Mylar membranes across the main performance criteria outlined in Sections 2 and 3. For each test, replicated trials are reported, average values are analyzed, and the observed differences are interpreted in relation to the requirements of small-scale LTA envelopes.

5.1. Density measurements

Helium pycnometer measurements confirmed that raw LDPE (48 g/m^2) was substantially lighter than PU (70 g/m^2) but heavier than Mylar (27.6 g/m^2). After coating, LDPE reached 54.5 g/m^2, representing a 13.5% increase relative to the uncoated film, yet it remained 22.1% lighter than PU (Table 3). This result indicated that the coating added marginal mass while preserving LDPE's weight advantage over PU.

These results show that the surface treatment preserves the low areal density of LDPE while providing improved gas barrier performance. In contrast to multilayer laminates or barrier films discussed in Section 2, which typically achieve enhanced gas retention through substantial weight increases, the proposed coating strategy delivers functional improvement without compromising mass efficiency.

5.2. Tear test

Tear resistance results (Fig. 10 a) showed LDPE as the strongest performer, averaging 5.62 ± 0.07 N, compared to PU (5.24 ± 0.08) N and

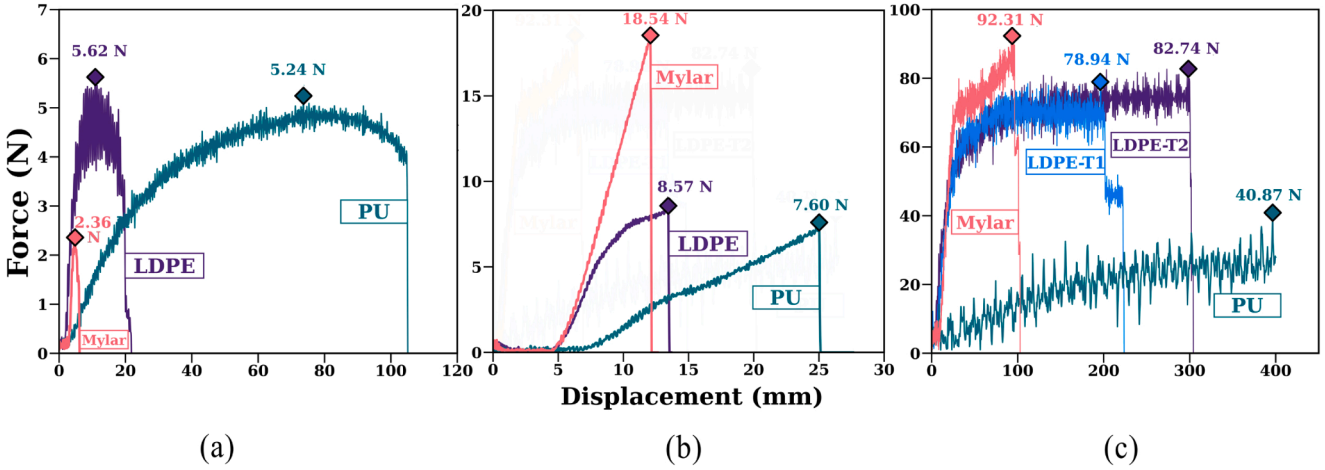

Fig. 10. Force–displacement curves from mechanical testing: (a) tear resistance, (b) puncture resistance, and (c) tensile strength of sealed joints. Curves are representative responses from repeated tests; the annotated peak values correspond to the mean of four specimens for each material/configuration.

Mylar (2.36 ± 0.14) N . LDPE thus exceeded PU by 9.1% and Mylar by 138.1%. The apparent fluctuations in Fig. 10a were attributed to electronic noise, since the measured load was small compared to the load cell capacity. These results highlighted LDPE's ability to withstand out-of-plane stresses and its clear advantage over Mylar, whose brittleness led to low tear resistance.

5.3. Puncture test

Puncture resistance values (Fig. 10 b) revealed a different hierarchy. Mylar withstood the highest force (18.54 ± 0.20) N, but failed at relatively low displacement (11 mm), indicating a stiff yet brittle response. PU, in contrast, failed at the lowest force (7.60 ± 0.27) N, but endured the largest displacement (25 mm), demonstrating ductility without high puncture strength. LDPE exhibited an intermediate behavior (8.57 ± 0.28) N at 13 mm, offering a balance between load capacity and deformation. The larger standard deviation observed for PU indicated greater variability under localized loading.

5.4. Tensile strength of welded joints

Across all configurations, failures occurred in the bulk material rather than at the joints, confirming that the thermal welding process produced interfaces stronger than the films themselves (Fig. 10 c). LDPE-T2 (flap joint) achieved the highest maximum load (82.74 ± 0.27) N, slightly above LDPE-T1 (78.94 ± 0.16) N, indicating that joint geometry influenced stress distribution. Mylar reached the highest absolute load (92.31 ± 0.29) N but fractured at low displacement, confirming its brittle character. PU exhibited the largest elongation (400 mm) but carried the lowest maximum load (40.87 ± 0.29) N, demonstrating ductility. The oscillations visible in the curves (Fig. 10 c) were attributed to a combination of stick-slip crack propagation, as previously reported for thin polymer films [45], and the large specimen extension (≈ 400 mm), which magnified displacement fluctuations during testing.

5.5. High specific strength

Normalizing the results by areal density (Table 4) provided insight into mechanical efficiency. Mylar achieved the best strength-to-weight performance in tensile and puncture tests, but its poor tear resistance and brittle failure undermined practical utility. LDPE provided the most balanced profile, offering moderate efficiency with superior tear resistance and ductility. PU, while flexible, underperformed in both normalized strength and permeability.

Table 4
Normalized strength-to-weight ratios for envelope materials (tear, puncture, and tensile performance), calculated as force (N) divided by surface density (g/m^2). The higher these values, the more mechanically efficient the material is for lightweight airship applications.

Metric (N·m^2/g)	LDPE	PU	Mylar
Tear Resistance	0.1171	0.0736	0.0855
Puncture Resistance	0.1781	0.1086	0.6725
Tensile Strength (Max Load)	1.723	0.584	3.345

5.6. Gas barrier test

Helium leakage tests (Fig. 11a) revealed Mylar as the most impermeable material, with a mean leakage rate of 0.14 g/h (98.5% lift retention over 6 h). LDPE exhibited intermediate performance (0.64 g/h, 93.6% retention), while PU performed the poorest (1.08 g/h, 84.5%). Reported values correspond to mean leakage rates obtained from repeated tests. When normalized, leakage rates were 0.84 g/h for Mylar, 3.8 g/h for LDPE, and 5.47 g/h for PU. Thus, coated LDPE retained 40.7% more lift than PU, confirming the effectiveness of the sol-gel coating.

Post-agitation tests (Fig. 11b) showed sharp degradation in Mylar, whose leakage rate increased eightfold (to 6.87 g/h) due to delamination of its aluminized layer. PU also worsened modestly (to 6.47 g/h), while LDPE remained stable (3.8 g/h), reflecting the resilience of both the polymer and the applied coating under repeated deformation.

Large-scale validation using a cylindrical envelope (Section 6) confirmed these trends (Fig. 11c). PU leaked at 4.2 g/h, while LDPE lost only 1.7 g/h, consistent with diffusion scaling by surface area. The results are consistent with the behavior reported in prior studies and with permeability trends summarized in Section 2 and Table 1, accounting for differences in surface area.

5.7. Wettability properties

Contact angle measurements (Fig. 12) confirmed that the coated LDPE surface was strongly hydrophobic (117.5°), surpassing PU (95.9°),

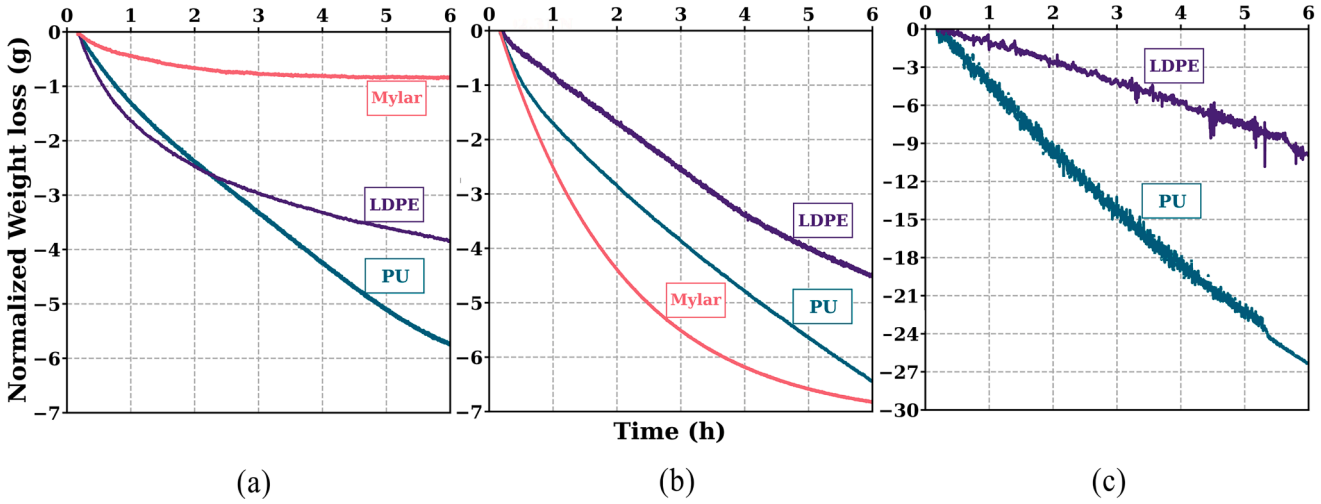

Fig. 11. Results of gas barrier tests: (a) Helium leakage rates of pillow-shaped envelopes fabricated from LDPE, Mylar, and PU; (b) leakage rates of the same samples after mechanical agitation in a dryer; and (c) leakage rates of full-scale LDPE and PU envelopes. For cases (a) and (b), curves represent mean values obtained from three repeated tests per material. Together, these results highlight the relative effectiveness of each material in limiting gas loss, a critical parameter for assessing their suitability in practical airship applications.

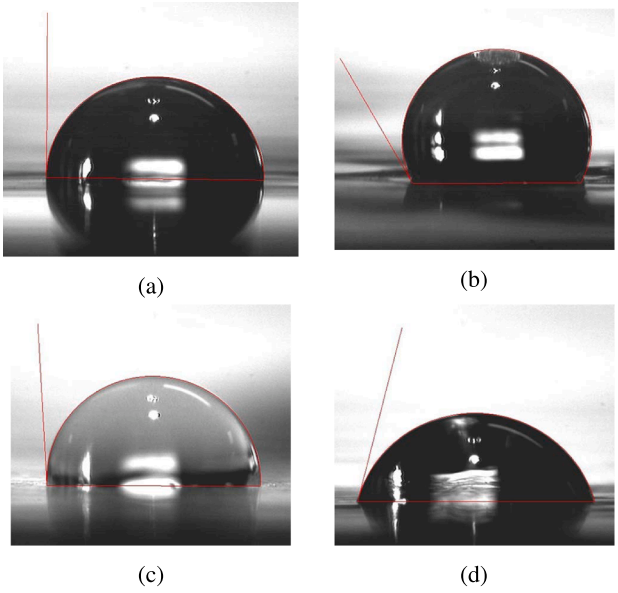

Fig. 12. Mean contact angles of various films, illustrating wettability: (a) Uncoated LDPE film (92.75° ± 1.38°), (b) Fluoro-siloxane sol-gel coated LDPE (117.53° ± 1.89°), (c) PU film (95.88° ± 1.44°), and (d) Mylar film (73.95° ± 1.35 °).

uncoated LDPE (92.8°), and Mylar (73.9°). The coating thus significantly improved LDPE's water repellency, reducing risks of mass gain or mechanical degradation under humid conditions.

5.8. Thermal welding test

Thermal welding trials highlighted clear differences in weldability among the materials. LDPE welded reliably at 170–175 °C, producing continuous weld seams with minimal deformation. PU was thermally welded at lower temperatures (110-125 °C with protective paper) but required tighter process control to avoid localized overheating. Mylar was thermally welded at 130–140 °C but was prone to wrinkling and distortion during manual handling, making fabrication more challenging. LDPE, therefore, demonstrated the widest tolerance to thermal welding conditions, supporting its use in semi-manual manufacturing.

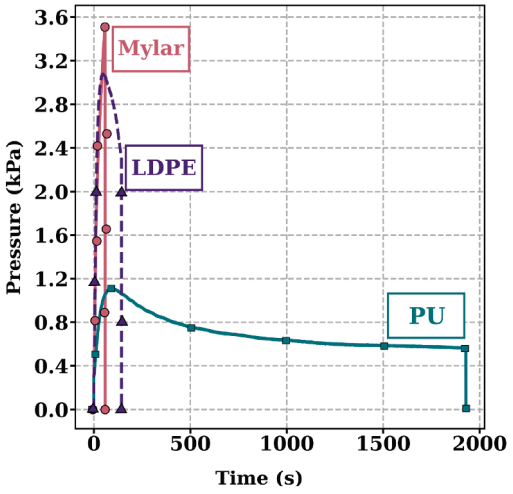

Fig. 13. Pressure-time profiles from biaxial inflation burst tests of Mylar, PU, and LDPE envelopes, illustrating inflation behavior and rupture progression under increasing internal pressure.

5.9. Validation of burt behavior

Burst tests (Figs. 13-14) revealed distinct rupture behaviors. Mylar reached the highest pressure (3.53 kPa) but failed explosively, with rupture initiating at the weld transition zone, reflecting stress concentration and its brittle nature. PU failed at the lowest pressure (1.11 kPa) after a prolonged plateau, consistent with ductile deformation and gradual leakage from the film body. LDPE withstood 3.08 kPa before rupture, failing in the bulk film rather than at welds. Its controlled, non-explosive rupture indicated a balance between strength and ductility, as well as reliable weld integrity.

6. Field demonstration

A deployment trial was conducted in a partially flooded cave environment[5], characterized by narrow passages and fragile surfaces that

[5] Montreal's Saint-Léonard Cave

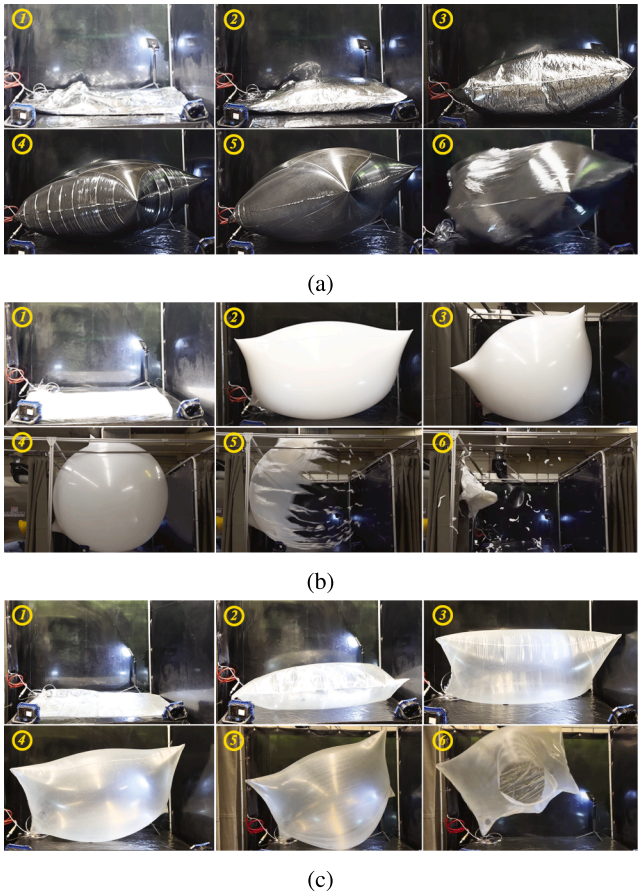

Fig. 14. Rupture sequences for inflated envelopes (1200 × 800 mm): (a) Mylar, (b) PU, and (c) LDPE. Sequences show key stages of inflation and rupture under biaxial loading, highlighting material-specific rupture initiation, failure modes, and tear propagation.

Table 5
Decision matrix for material selection, comparing LDPE, PU, and Mylar across key parameters. Final ranking indicates overall performance for specific applications.

Technical Requirement	LDPE	PU	Mylar	Weight (%)
Density (g/m^2)	48 (4)	70 (2)	27.60 (5)	20%
Thickness (mm)	0.0498 (5)	0.0524 (4)	0.0256 (2)	8%
Tear Resistance (N)	5.62 (5)	5.15 (4)	2.36 (2)	15%
Puncture Resistance (N)	8.57 (3)	7.60 (2)	18.54 (5)	5%
Tensile Strength (N)	82.74 (4)	40.87 (2)	92.34 (5)	15%
Gas Barrier Performance (Leakage rate)	0.64 (4)	1.08 (3)	0.14 (5)	15%
Lift Retention (%)	93.60 (4)	84.50 (2)	98.50 (5)	10%
Hydrophobicity (CA)	117.53° (5)	92.75° (2)	95.88° (2)	5%
Burst Pressure (Structural Integrity)	3.08 (5)	1.11 (4)	3.53 (1)	5%
Reusable	High (5)	High (5)	Low (1)	2%
Final Rank	**4.5**	**2.77**	**3.88**	100%

precluded direct human exploration. The objective was to assess the capacity of an autonomous scout airship to operate reliably in confined, humid, and high-risk conditions.

In Table 5, for each criterion, the value in parentheses is a normalized rating on a 1-5 scale (5 = best performance, 1 = poorest), assigned by comparing the measured results of LDPE, PU, and Mylar. Based on this decision matrix, the comparative analysis of laboratory results identified coated LDPE as the most suitable candidate for envelope fabrication, achieving the highest weighted score (4.50) compared to Mylar (3.88) and PU (2.77). Although Mylar exhibited excellent helium retention, its low tear resistance, limited durability, and lack of reusability and sustainability disqualified it as a candidate, despite its higher score relative to PU. PU, while disadvantaged by high mass and rapid gas loss, was retained as a benchmark due to its robustness, demonstrated reusability, and established use in industrial practice. Coated LDPE provided the most balanced performance, combining durability, barrier properties, low weight, and hydrophobicity. Consequently, coated LDPE and PU were selected for full-scale field validation. The LDPE envelope was fabricated following the protocol in sec. 4 and was compared with an industrially manufactured PU envelope of identical geometry (Fig. 15).

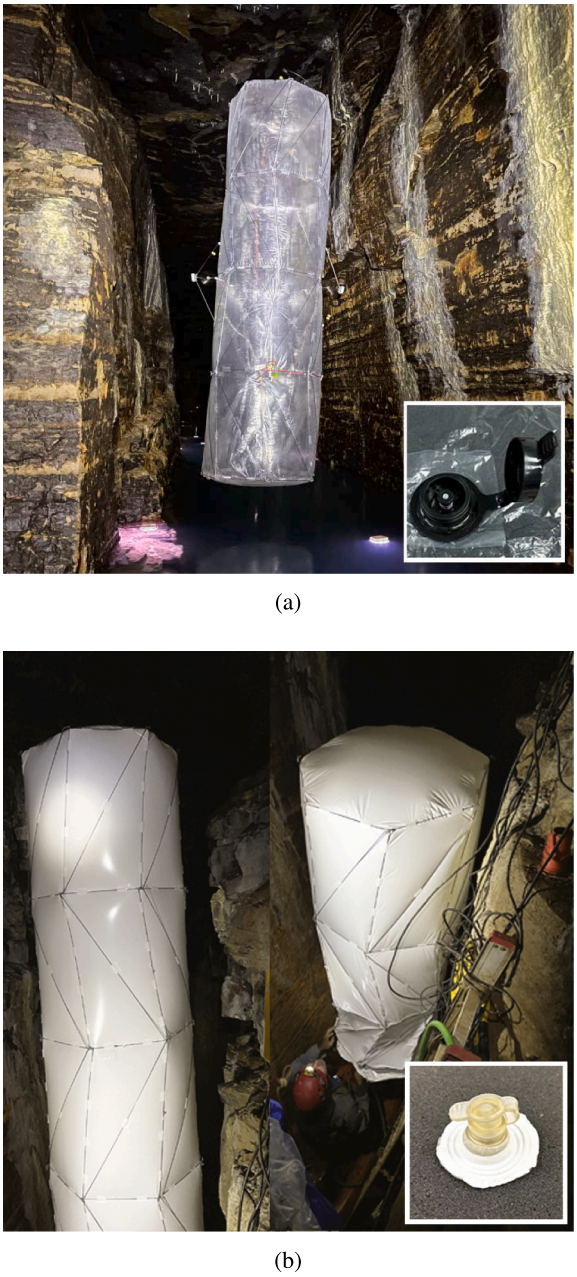

Fig. 15. Envelope performance during a mission in a cave environment: (a) LDPE envelope with a one-way valve assembled in the laboratory, and (b) PU envelope.

The most significant difference between the two materials was observed in their final envelope mass, which resulted from intrinsic material density. The LDPE envelope was lighter, thereby preserving a larger payload margin. This additional margin allowed the integration of a more secure, though heavier, valve assembly. Even with the inclusion of a heavier valve system (20.74 g including a 7 g cap), the coated LDPE

Table 6
Performance parameters for single-body indoor airships made from LDPE and PU, highlighting key metrics for material suitability.

Parameter	LDPE	PU
Envelope Volume (m^3)	0.86	0.86
Rigid Skeleton Weight (g)	215	215
Avionic Weight (g)	223.62	223.62
Envelope Weight (Non-Coated LDPE) (g)	325	401
Envelope Weight (Coated LDPE) (g)	343	401
Airship Free Payload Capacity (g)	250	164
Helium Loss Rate (g/h)	1.7	4.2
Moisture Absorption	None	High
Operational Endurance (hours)	72	24

envelope remained at 343 g, lighter than the PU envelope at 401 g. The coating applied to the LDPE contributed only 3 g/m^3 of additional mass, a negligible increase that remained well within operational tolerances and did not compromise payload capacity. Although it was technically feasible to employ the same one-way valve on PU, such an option has not been adopted in industrial practice, as the additional weight would have exacerbated PU's high mass, thereby reducing available payload.

The results confirmed the laboratory findings and underscored LDPE's advantages in practical operation (Table 6). The LDPE envelope sustained a payload capacity of 250 g, significantly higher than the 164 g supported by PU, allowing the integration of both lidar and micro-camera sensors with additional mass margin for leakage compensation.

Gas retention was markedly superior: the LDPE vehicle remained inflated for several days without refilling, whereas the PU envelope required replenishment twice a day. Under humid conditions, PU absorbed moisture, increasing weight and necessitating intermittent drying, while LDPE maintained stable mass and flight behavior due to its hydrophobic surface. Deployment time was also reduced: the LDPE envelope could be prepared in approximately 15 minutes, facilitated by an integrated one-way valve, compared to 25 minutes for PU using manufacturer-supplied fittings. In terms of overall endurance, the LDPE airship sustained continuous flight for 72 hours before requiring intervention, representing a threefold improvement over the 24-hour operational lifespan of the PU envelope.

Taken together, these results validated coated LDPE as a robust alternative to conventional materials for indoor airship platforms. Its combination of lightweight structure, durability under mechanical stress, moisture resistance, and superior helium retention enabled extended mission duration in confined or humid environments, confirming its relevance for next-generation LTA systems designed for exploration and monitoring in inaccessible spaces.

7. Conclusion

This study developed and validated a coated LDPE composite film as an engineered solution for lightweight, gas-tight, and durable envelopes for LTA systems operating in confined spaces. By combining a thin LDPE film with a fluoro-siloxane sol-gel coating, the design achieved a balance between low surface density, high tear resistance, and improved helium retention. Comprehensive laboratory tests demonstrated that coated LDPE rivaled or exceeded the performance of conventional PU and Mylar films across key metrics, while maintaining superior flexibility, hydrophobicity, and compatibility with semi-manual thermal welding processes.

A field demonstration in a partially flooded cave further confirmed the composite film's practical viability, enabling higher payload capacity, easier deployment, and up to threefold longer flight endurance compared to PU. These findings not only established the coated LDPE film as a reliable structural-functional composite for indoor airships but also illustrated a generalizable materials-engineering pathway for lightweight polymer composites in soft robotic and aerospace applications.

Future work will extend this approach toward scalable manufacturing, optimization of envelope geometry to reduce seam length, and assessment under long-term or outdoor operation. In addition, future work will be required to quantitatively validate and characterize the anisotropy of LDPE. These efforts will further consolidate coated LDPE as a versatile material for persistent aerial exploration in complex environments.

CRediT authorship contribution statement

Afsaneh Kheirani: Writing - review & editing, Writing - original draft, Visualization, Validation, Software, Methodology, Investigation, Data curation, Conceptualization; **Ilyass Tabiai:** Writing - review & editing, Validation, Supervision, Methodology; **David St-Onge:** Writing - review & editing, Validation, Supervision, Resources, Project administration, Investigation, Funding acquisition, Conceptualization.

Data availability

All data supporting the findings of this study are available within the article.

Declaration of competing interest

The authors declare that they have no known competing financial interests or personal relationships that could have appeared to influence the work reported in this paper.

Acknowledgments

We would like to thank the Fonds de recherche du Québec – Nature et technologies (FRQNT) for their financial support (Team grant #283381), which made this work possible.

References

[1] P.S. Agrawal, et al., Advancements and challenges in drone technology: a comprehensive review, in: 2024 4th International Conference on Pervasive Computing and Social Networking (ICPCSN), 2024. Available online (accessed October 2, 2025).
[2] S. Awasthi, et al., Micro UAV swarm for industrial applications in indoor environment: a systematic literature review, Logist. Res. 16 (1) (2023) 1–43. https://doi.org/10.1007/s12159-023-01002-8
[3] P. Nooralishahi, et al., Drone-based non-destructive inspection of industrial sites: a review and case studies, Drones 5 (4) (2021) 106. https://doi.org/10.3390/drones5040106
[4] A.R. Qubaa, A.N. Hamdon, T.A. Al Jawwadi, Morphology detection in archaeological ancient sites by using UAVs/drones data and GIS techniques, Iraqi J. Sci. 62 (11 (SI)) (2021) 4557–4570. https://doi.org/10.24996/ijs.2021.62.11(SI).35
[5] R.S. Pahwa, et al., Dense 3D reconstruction for visual tunnel inspection using unmanned aerial vehicle, in: 2019 IEEE/RSJ International Conference on Intelligent Robots and Systems (IROS), IEEE, 2019, pp. 5128–5133. https://doi.org/10.1109/IROS40897.2019.8967577
[6] K. Themistocleous, The use of UAVs for cultural heritage and archaeology, in: Handbook of Research on Emerging Technologies for Digital Preservation and Information Modeling, Advances in Science, Technology & Innovation, Springer, 2019, pp. 297–319. https://doi.org/10.1007/978-3-030-10979-0_14
[7] A. Maity, S. Majumder, D.N. Ray, Amphibian subterranean robot for mine exploration, in: 2013 International Conference on Robotics, Biomimetics, Intelligent Computational Systems, IEEE, 2013, pp. 65–70. https://doi.org/10.1109/ROBIONETICS.2013.6743612
[8] J.E. Salas Gordoniz, N. Reeves, D. St-Onge, Modular foldable airship concept for subterranean exploration, in: Proceedings of the ASME International Design Engineering Technical Conferences (IDETC), 85451, American Society of Mechanical Engineers, 2021, pp. V08BT08A018–1–V08BT08A018–9. https://doi.org/10.1115/DETC2021-69954
[9] L. Escobar, G.A.S. Pereira, Energy-aware coverage path planner for multirotor UAVs, in: 2025 International Conference on Unmanned Aircraft Systems (ICUAS), IEEE, 2025. Available online (accessed October 2, 2025).
[10] T. Sands, Autonomous real-time mass center location and inertia identification for grappling space robotics, Technologies 13 (4) (2025) 148. https://doi.org/10.3390/technologies13040148

[11] N. Mandlekar, M. Joshi, B.S. Butola, A review on specialty elastomers based potential inflatable structures and applications, Adv. Industr. Eng. Polymer Res. 5 (1) (2022) 33–45. https://doi.org/10.1016/j.aiepr.2021.05.004
[12] L. Liao, I. Pasternak, A review of airship structural research and development, Prog. Aerosp. Sci. 45 (4-5) (2009) 83–96. https://doi.org/10.1016/j.paerosci.2009.03.001
[13] S.S. Mulay, R.S. Pant, Design, fabrication and flight testing of a non-rigid indoor airship, AIAA Lighter-Than-Air Syst. Technol. Conf. Proceed. 2013 (1) (2013) 1–9. https://doi.org/10.2514/6.2013-1297
[14] M. Biju, R.S. Pant, Design and development of an indoor autonomous airship, AIAA Lighter-Than-Air Syst. Technol. Conf. Proceed. 2017 (1) (2017) 1–8. https://doi.org/10.2514/6.2017-3996
[15] h. Shoeb, Design and development of an easily deployable indoor finless airship, International Conference on Advances in Robotics, Mechanical Engineering and Automation (2017) 1–6.
[16] G. Gorjup, M. Liarokapis, A low-cost, open-source, robotic airship for education and research, IEEE Access 8 (1) (2020) 70713–70721. https://doi.org/10.1109/ACCESS.2020.2986772
[17] F.Mathieu, (2015) Un cube flottant dans la Verna: histoire d'une singulière grotte, 2015. Accessed on October 2, 2025
[18] D. St-Onge, N. Reeves, C. Gosselin, et al., Control, localization and human interaction with an autonomous lighter-than-air performer, Rob. Auton. Syst. 88 (1) (2017) 165–186. https://doi.org/10.1016/j.robot.2016.10.013
[19] A. Li, R. Vallabh, P.D. Bradford, D. Kim, A.F. Seyam, Development of hull material for high-altitude airship: a parametric study, J. Reinf. Plast. Compos. 41 (11-12) (2022) 444–458. https://doi.org/10.1177/07316844211054852
[20] A. Dhawan, P. Jindal, A review on use of polyurethane in lighter-than-air systems, Mater. Today Proc. 43 (2021) 746–752. https://doi.org/10.1016/j.matpr.2020.12.962
[21] S. Maekawa, K. Shibasaki, T. Kurose, T. Maeda, Y. Sasaki, T. Yoshino, Tear propagation of a high-performance airship envelope material, J. Aircr. 45 (5) (2008) 1546–1553. https://doi.org/10.2514/1.32264
[22] J. Bai, J. Xiong, X. Cheng, Tear resistance of orthogonal Kevlar-PWF-reinforced TPU film, Chin. J. Aeronaut. 24 (1) (2011) 113–118. https://doi.org/10.1016/S1000-9361(11)60014-9
[23] H.E. Barry, Ground-Handling systems for cargo airships, in: 52nd Annual Meeting Proceedings: Canadian Transportation Research Forum, 2017. Accessed on October 2, 2025.
[24] P. Nguyen-Tri, T.A. Nguyen, P. Carriere, C. Ngo Xuan, Nanocomposite coatings: preparation, characterization, properties, and applications, Int. J. Corros. 2018 (2018) 4749501. https://doi.org/10.1155/2018/4749501
[25] K. Majeed, R. Arjmandi, A. Hassan, Mechanical and oxygen barrier properties of LDPE/MMT/MAPE and LDPE/MMT/EVA nanocomposite films: a comparison study, J. Phys. Sci. 29 (1) (2018) 77–88. https://doi.org/10.21315/jps2018.29.1.4
[26] H. Zhai, A. Euler, Material challenges for lighter-than-air systems in high altitude applications, AIAA 5th ATIO and 16th Lighter-than-Air Sys Tech. and Balloon Systems Conferences (2005). https://doi.org/10.2514/6.2005-7488
[27] R. Vallabh, et al., Ultra-lightweight fiber-reinforced envelope material for high-altitude airship, J. Textile Inst. 113 (9) (2022) 1799–1805. https://doi.org/10.1080/00405000.2021.1948695
[28] Y.-L. Zhang, H. Xia, E. Kim, H.-B. Sun, Recent developments in superhydrophobic surfaces with unique structural and functional properties, Soft Matter 8 (44) (2012) 11217–11231. https://doi.org/10.1039/C2SM26517F
[29] X. Huang, N. Tepylo, V. Pommier-Budinger, M. Budinger, E. Bonaccurso, P. Villedieu, L. Bennani, A survey of icephobic coatings and their potential use in a hybrid coating/active ice protection system for aerospace applications, Prog. Aerosp. Sci. 105 (2019) 74–97. https://doi.org/10.1016/j.paerosci.2019.01.002
[30] S. Chouhan, S. Ghosh, B.S. Butola, M. Joshi, Studies of high-performance fabric-based laminated hull material for stratospheric airship, J. Reinf. Plast. Compos. 43 (17-18) (2024) 1008–1023. https://doi.org/10.1177/07316844231198301
[31] M. Joshi, B. Adak, B.S. Butola, Polyurethane nanocomposite based gas barrier films, membranes and coatings: a review on synthesis, characterization and potential applications, Prog. Mater. Sci. 97 (2018) 230–282. https://doi.org/10.1016/j.pmatsci.2018.05.001
[32] G. Bansal, U. Bhardwaj, N. Jain, S.S. Mulay, S. Sawardekar, R.S. Pant, Design fabrication and flight testing of a non-rigid indoor airship, AIAA Lighter-Than-Air Syst. Technol. (LTA) Conf. (2013). https://doi.org/10.2514/6.2013-1297
[33] N.I. Motiwala, I.A. Khan, N.P. Yelve, B.E. Narkhede, R.S. Pant, Conceptual approach for design, fabrication and testing of indoor remotely controlled airship, Adv. Mat. Res. 690 (2013) 3390–3395.
[34] R.F. Verheul, J. Breukels, W.J. Ockels, Material selection and joining methods for the purpose of a high-altitude inflatable kite, in: Proceedings of the Structures, Structural Dynamics, and Materials Conference, 2009. https://doi.org/10.2514/6.2009-2338
[35] A. Blanchard, F. Gouanvé, E. Espuche, Effect of humidity on mechanical, thermal and barrier properties of EVOH films, J. Memb. Sci. 540 (2017) 1–9. https://doi.org/10.1016/j.memsci.2017.06.031
[36] S. Collins, et al., The thermal stability of some vinylidene chloride copolymers, Polym. Degrad. Stab. 66 (1) (1999) 87–94. https://doi.org/10.1016/S0141-3910(99)00056-7
[37] M. Safandowska, C. Makarewicz, A. Rozanski, Tuning barrier properties of low-density polyethylene: impact of amorphous region nanostructure on gas transmission rate, Molecules 29 (20) (2024) 4950. https://doi.org/10.3390/molecules29204950
[38] W. Song, Z. Li, Y. Li, H. You, P. Qi, F. Liu, D.A. Loy, Facile sol-gel coating process for anti-biofouling modification of poly (vinylidene fluoride) microfiltration membrane based on novel zwitterionic organosilica, J. Memb. Sci. 550 (2018) 266–277. https://doi.org/10.1016/j.memsci.2017.12.076
[39] Shamini, G., Yusoh, K., 2014. Gas permeability properties of thermoplastic polyurethane modified clay nanocomposites. Int. J. Chem. Eng. Appl. 5, 64–68. https://doi.org/10.7763/IJCEA.2014.V5.352
[40] K. Xu, Y. Wen, X. Xu, Melt flow ratio: a way to identify the type of polyethylene, Adv. Industr. Eng. Polymer Res. 6 (1) (2023) 79–82. https://doi.org/10.1016/j.aiepr.2022.08.001
[41] C. Changyi, Exploring alternative Functional Thin Layers (FTL's) for high tear packaging applications, Master's thesis, KTH Royal Institute of Technology. Accessed on October 2, 2025, (2024)
[42] M. Seifali Abbas-Abadi, M. Nekoomanesh Haghighi, H. Yeganeh, Effect of the melt flow index and melt flow rate on the thermal degradation kinetics of commercial polyolefins, J. Appl. Polym. Sci. 126 (5) (2012) 1739–1745. https://doi.org/10.1002/app.36775
[43] ASTM International, 2023. ASTM D1238-23a: Standard Test Method for Melt Flow Rates of Thermoplastics by Extrusion Plastometer. ASTM International, West Conshohocken, PA, USA.
[44] ASTM International, ASTM-D1004-21:Standard Test Method for Tear Resistance of Plastic Film and Sheeting, 2021, Accessed on October 2, 2025
[45] h. Eskil, Trouser tear tests of two thin polymer films, in: 13th International Conference on Fracture (ICF13), 2013. Accessed on October 2, 2025.
[46] ASTM International, ASTM F1306-21: Standard test method for slow rate penetration resistance of flexible barrier films and laminates, 2021, Accessed on October 2, 2025.
[47] ASTM International, ASTM F88/F88M-21: Standard Test Method for Seal Strength of Flexible Barrier Materials, 2021, Accessed on October 2, 2025.
[48] R.S. Pant, Design, fabrication and flight demonstration of a remotely controlled airship for snow scientists, J. Aerosp. Technol. Manage. 6 (1) (2014) 19–27. https://doi.org/10.5028/jatm.v6i1.313
[49] X. The Moonshot Factory, (2014) Loon Project Collection, 2024. Accessed on October 2, 2025.
[50] J.L. Hall, J.A. Jones, B. Clark, J.A. Cutts, R.E. Young, D. Crisp, Second generation prototype design and testing for a high altitude venus balloon, Adv. Space Res. 44 (1) (2009) 93–105. https://doi.org/10.1016/j.asr.2008.10.033
[51] S. Li, L. Chen, Y. Song, X. Mi, W. Chen, H. Zhao, Pressure-bearing performance of sliding poly-*p*-phenylene benzobisoxazole-rope-reinforced spherical composite envelope structures, Thin-Walled Struct. 180 (2022) 109929. https://doi.org/10.1016/j.tws.2022.109929
[52] Y. Chen, W. Yang, W. Xie, X. Wang, G. Fu, Meso-Scale tearing mechanism analysis of flexible fabric composite for stratospheric airship via experiment and numerical simulation, J. Shanghai Jiaotong University (Science) 27 (6) (2022) 873–884. https://doi.org/10.1007/s12204-022-2431-8
[53] S. Li, W. Chen, L. Chen, Y. Song, J. Hu, H. Zhao, D. Zhang, Experimental study and refined numerical simulation of ultimate pressure-bearing performance of rope-reinforced airship envelope structures, Adv. Struct. Eng. 27 (7) (2024) 1266–1282. https://doi.org/10.1177/13694332241246376
[54] A. Gawale, A. Raina, R. Pant, Y. Jahagirdar, Design, fabrication and operation of remotely controlled airships in India, in: 18th AIAA Lighter-Than-Air Systems Technology Conference, 2009, p. 2855. https://doi.org/10.2514/6.2009-2855
[55] C. Louis, I. Tabiai, D. St-Onge, CAVERNAUTE: A design and manufacturing pipeline of a rigid but foldable indoor airship aerial system for cave exploration, arXiv preprint (2024). arXiv:2409.07591.
[56] M.R. Sanchis, M. Blanes, O. Fenollar, D. Garcia, R. Balart, Surface modification of low density polyethylene (LDPE) film by low pressure O2 plasma treatment, Eur. Polym. J. 42 (7) (2006) 1558–1568. https://doi.org/10.1016/j.eurpolymj.2006.02.001
[57] J.-S. Kong, D.-J. Lee, H.-D. Kim, Surface modification of low-density polyethylene (LDPE) film and improvement of adhesion between evaporated copper metal film and LDPE, J. Appl. Polym. Sci. 82 (7) (2001) 1677–1690. https://doi.org/10.1002/app.2008